Journal Pre-proof

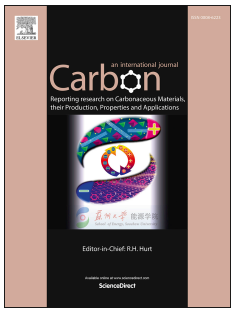

Fractal-seaweeds type functionalization of graphene

Konstantin Amsharov, Dmitry I. Sharapa, Oleg A. Vasilyev, Martin Oliver, Frank Hauke, Andreas Goerling, Himadriben Soni, Andreas Hirsch

PII: S0008-6223(19)31132-7

DOI: https://doi.org/10.1016/j.carbon.2019.11.008

Reference: CARBON 14765

To appear in: *Carbon*

Received Date: 7 July 2019

Revised Date: 17 October 2019

Accepted Date: 3 November 2019

Please cite this article as: K. Amsharov, D.I. Sharapa, O.A. Vasilyev, M. Oliver, F. Hauke, A. Goerling, H. Soni, A. Hirsch, Fractal-seaweeds type functionalization of graphene, *Carbon* (2019), doi: https://doi.org/10.1016/j.carbon.2019.11.008.

HOSTED BY
ELSEVIER

Available online at www.sciencedirect.com

Carbon

Journal homepage: www.elsevier.com/locate/rgo

Fractal-Seaweeds Type Functionalization of Graphene

Konstantin Amsharov*[a,b], Dmitry I. Sharapa[c], Oleg A. Vasilyev[d,e], Oliver Martin[a], Frank Hauke[a], Andreas Goerling[f], Himadriben Soni[f] and Andreas Hirsch*[a]

[a] Friedrich-Alexander University Erlangen-Nuremberg, Department of Chemistry and Pharmacy, Organic Chemistry II, Nikolaus-Fiebiger Str. 10, 91058 Erlangen, Germany
[b] South Ural State University, pr. Lenina 76, 454080 Chelyabinsk, Russia
[c] Institute of Catalysis Research and Technology, Karlsruhe Institute of Technology (KIT), Herrmann-von-Helmholtz-Platz 1, 76344 Eggenstein-Leopoldshafen, Germany
[в] Max Planck Institute for Intelligent Systems, Heisenbergstrasse 3, D-70569 Stuttgart, Germany
[e] Institute for Theoretical Physics IV, University Stuttgart, Pfaffenwaldring 57, D-70569 Stuttgart, Germany
[f] Friedrich-Alexander University Erlangen-Nuremberg, Department of Chemistry and Pharmacy, Theoretical Chemistry, Egerland Str.3, 91058 Erlangen, Germany

ARTICLE INFO

Article history:
Received 00 December 00
Received in revised form
00 January 00
Accepted 00 February 00

Keywords:
graphene
functionalization
regioselectiviy
topicity

ABSTRACT

In this work, we present a systematic investigation on the regioselectivity and topicity of radical hydrogenation/alkylation of graphene. The complex process of sequential covalent binding of hydrogen and methyl radicals to the edges and basal plane of graphene, and addition to the direct neighborhood of pre-existing defects were quantitatively investigated using different computational techniques. Considering both thermodynamic and kinetic factors a general model for graphene functionalization has been developed. Based on the proposed model we performed numerical Monte-Carlo simulations, which provide evidence of a fractal expansion of functionalized regions leading to a fractal-seaweeds type of addition. We show that the applications of the model is widespread and includes the description of Birch-like hydrogenation, reductive alkylation and direct radical addition, which allows to evaluate the effect of the size, shape and the quality of a graphene flake on the addition morphology.

* *Corresponding author.*
Tel. +49 913185 65581,
E-mail address: *konstantin.amsharov@fau.de*, *andreas.hirsch@fau.de*

1. Introduction

Graphene, is a single-atom-thick sheet of sp^2-hybridized carbon atoms arranged in a hexagonal lattice, representing the thinnest and strongest 2D-material.[1] Among outstanding mechanical properties, graphene is an excellent conductor of heat and electricity.[2-5] Due to an unique set of properties this carbon allotrope is currently considered as the most promising material for the future post-silicon electronics.[6] On the other hand, pristine graphene itself is a semimetal with a zero band gap, which is disadvantageous for application in functional electronic devises. In this context, the chemical functionalization of graphene represents the most facile approach to open and tune a band gap.[7-12] However, due to low reactivity of the graphene surface the chemistry of graphene is rather difficult to tackle.[13-19] Among a broad variety of methods for covalent graphene functionalization, alkylations and arylations *via* reductively activated graphite and Birch-type hydrogenations appear to be the most versatile and mild methods offering a large product scope and control over the degrees of functionalization.[20-23] Among efficient exfoliation of graphene sheets, this approach allows for bulk production of high-quality single-layer graphene with very high surface-to-mass ratio. Depending on the type of electrophiles used, this route enables facile access to alkylated,[16, 17] arylated,[17] and hydrogenated,[20, 24] graphene derivatives. However, detailed information about the topicity, regiochemistry and homogeneity of sequential addend binding are still scarce. The main reason for this lack of knowledge is the difficulty in characterizing the reaction products, because the common structure elucidation tools, such as NMR spectroscopy and mass spectrometry, usually cannot be applied to these polydisperse and rather insoluble materials. As a consequence, non-classical and more indirect analytic methods such as Raman spectroscopy, thermogravimetric analysis coupled with gas chromatography/mass spectrometry and high resolution microscopy are required for product characterization.[13, 25-28] As a result, the exact nature of covalent addend distribution of the graphene surfaces which dictates the electronic properties remains almost completely unexplored. To the best of our knowledge this important question has never been properly addressed in the literature and structural models were only proposed for the graphene oxide systems. [29]

In this contribution, we present a systematic investigation on the regioselectivity and topicity of

multiple covalent addend binding to graphene. Our study is based on extended quantum mechanical calculations, stochastic growth simulations and comparison with previously collected experimental data. To shine light on the regiochemistry of covalent addend binding we quantitatively investigated sequential radical attachments to graphene, including addition to the basal plane and edges of pristine graphene and addition to the direct neighborhood of pre-existing defects. Detailed consideration of both thermodynamically and kinetically controlled processes, allows us to propose a general model describing the graphene reactivity. Based on the proposed model we perform numerical Monte-Carlo simulations of addend binding which provides evidence of a fractal expansion of "defects" leading to a fractal-seaweeds type of addition. The data obtained not only provide deep understanding of the process of graphene functionalization but also open a venue for the rational control of this complex process.

2. Results and discussions

2.1. Birch reduction

The Birch reduction is a classic method for hydrogenation of aromatic molecules in liquid ammonia with earth alkaline metals such as sodium, lithium or potassium in the presence of an alcohol as a proton donor.[30, 31] This reaction has numerous variations that expand its scope far beyond the reduction of small aromatics. Thus, it has been shown that graphite can be effectively hydrogenated under Birch-like conditions yielding partially hydrogenated graphene.[19, 24, 32, 33] Interestingly that for graphene hydrogenation water (in the form of ice) was found to be the best proton donor agent.[13, 15, 17, 19] Recently, the scope of the Birch-type reduction has been extended to the direct hydrogenation of graphene flakes on SiO_2/Si substrates.[23, 34, 35] Although the Birch-type reduction of graphene is rather well developed, a detailed characterization of the final products, including distribution pattern of hydrogen, has yet to be established. The mechanism of the Birch reduction is firmly understood for small aromatics and small polycyclic aromatic hydrocarbons (PAHs),[36] and expected to be rather similar for large PAH systems including nanographenes and graphene.

2.2. Birch-type hydrogenation of grapheme

As it will be shown below on the base of high-level quantum chemical calculation, the graphene chemistry can be easily rationalized in the term of localized aromatic sextets or the so called Clar's

sextets. [37, 38] According to Clar's rule, for a given molecule, the representation with a maximum number of sextets of electrons, called the Clar formula, is the most representative one. The Clar formula predict the properties of PAHs such as the bond length alternations, the local density of π-states as well as PAH reactivity. In fact, for many PAHs it has been reported that the aromatic rings in terms of NICS (nuclear independent chemical shift) correspond to Clar's π-sextets.[39-41] The Clar's concept (supported by the high-level quantum chemical calculations) will serve here as a central concept in the rationalisation of graphene chemistry and is a basis of the proposed graphene functionalization model.

We will first consider the hydrogenation of the periphery of a graphene sheet, which is known to be more reactive than the basal plane.[42] The most likely scenario of the single Birch-type hydrogenation of graphene is schematically presented in **Scheme 1**. According to the accepted mechanism, the electropositive metal provides electrons that are transferred to the conjugated π-system of graphene **1** forming the corresponding radical anion **2**. Formally, the anion and radical centres in **2** are delocalized over the whole π-system of a graphene. Thus, each carbon atom in graphene is potentially activated for the protonation. The resonance structure of **2** depicted in **Scheme 1** represents one of the energetically more favourable situations, where both centres are localized in the same hexagon. Note the respective resonance structures obey the Clar rule and possess the maximal number of localized Clar's sextets. The electron transfer is then followed by protonation to form a cyclohexadienyl-type radical **3**. In accordance with Clar's rule, this step causes "fixation" of the radical position within the respective hydrogenated hexagon as it is shown in **Scheme 1**. It is worth mentioning that these reactive free radical intermediates can undergo rearrangements *via* a hydrogen shift forming the most stable radical.[43, 44] Thus, for example, **3** is expected to rearrange to the more stable radical **5** *via* a fast 1,2-hydrogen shift. The possibility of the rearrangement in radical intermediates appear to be a key prerequisite which determine the regioselectivity of the hydrogenation process and will be discussed later in more detail. The second electron transfer to the radical **5** yields a cyclohexadienyl carbanion **7**. In the final step a second hydrogen addition yields adduct **8**. Three isomeric products can be expected in this case, since three nucleophilic centers are available for attack, namely compound **8a** (1,4 addition) and compounds **8b** and **8c** (1,2 addition). Independent of the hydrogenation position, all regioisomers contain the maximum number of Clar's sextets since only one aromatic "benzene" fragment is "affected" as it is schematically depicted for structure **8**. Note that

small monocyclic aromatics typically undergo selective 1,4-additions, whereas PAHs can undergo both 1,2- and 1,4-addition depending on the PAH structure. PAHs in general are considerably more reactive compounds than monocyclic benzenes.[45, 46] In contrast to benzenes derivatives, PAHs can easily accept a second electron yielding the corresponding dianions. Subsequently, extra-large π-systems such as nanographenes and graphene can accommodate very large numbers of electrons leading to multiply charged targets. We do not exclude the influence of the multi charged character of graphene on its reactivity. However, it is reasonable to assume that Coulomb interactions will prevent the charge localisation. Therefore, mono- and di- anionic systems appears to be suitable models for the investigation of the hydrogenation mechanism. Thus, the anion-radical **2** can readily accept a second electron forming an anion such as **6**. Similar to PAHs the subsequent protonation is expected to proceed easily generating the most stable monoanion.[43] It is important to mention, that anions cannot undergo 1,2-hydrogen shift which would require a four-electron antiaromatic transition state. Thus, direct rearrangement of **6** to **7** is highly unlikely. However, this transformation can be imagined *via* electron-hole catalysis,[42] which explains the experimentally determined correlation between anion stability and the regioselectivity of addition.[43] As shown in **Scheme 1** the equilibrium between dianion **6** and **7** can be realised *via* the anion radicals **3** and **5**. Thus, although several paths of hydrogenation are possible (*via* radical anion, dianion or multi charged species) they are all expected to lead to the formation of the same product **8**. It is worth to mention that due to heterogeneous character and multicharged nature, the real process of graphene reduction expected to be more complex than discussed above mechanism. However, independent of the complexity and reaction condition the stability of the intermediate radical should play a major role in the regioselectivity of the process. Moreover, the direct radical hydrogenation should result in the formation of exactly the same intermediates (**3** and **5**) and finally lead to the same product (**8**). Thus, in a first approximation the hydrogen radical addition can be used as a simplified model for describing of the complex reductive addition, independent of the exact mechanism of the reaction. As it is shown in **Scheme 1** the direct radical hydrogenation (highlighted by blue) yields the same radical intermediates and finally leads to essentially the same outcome.

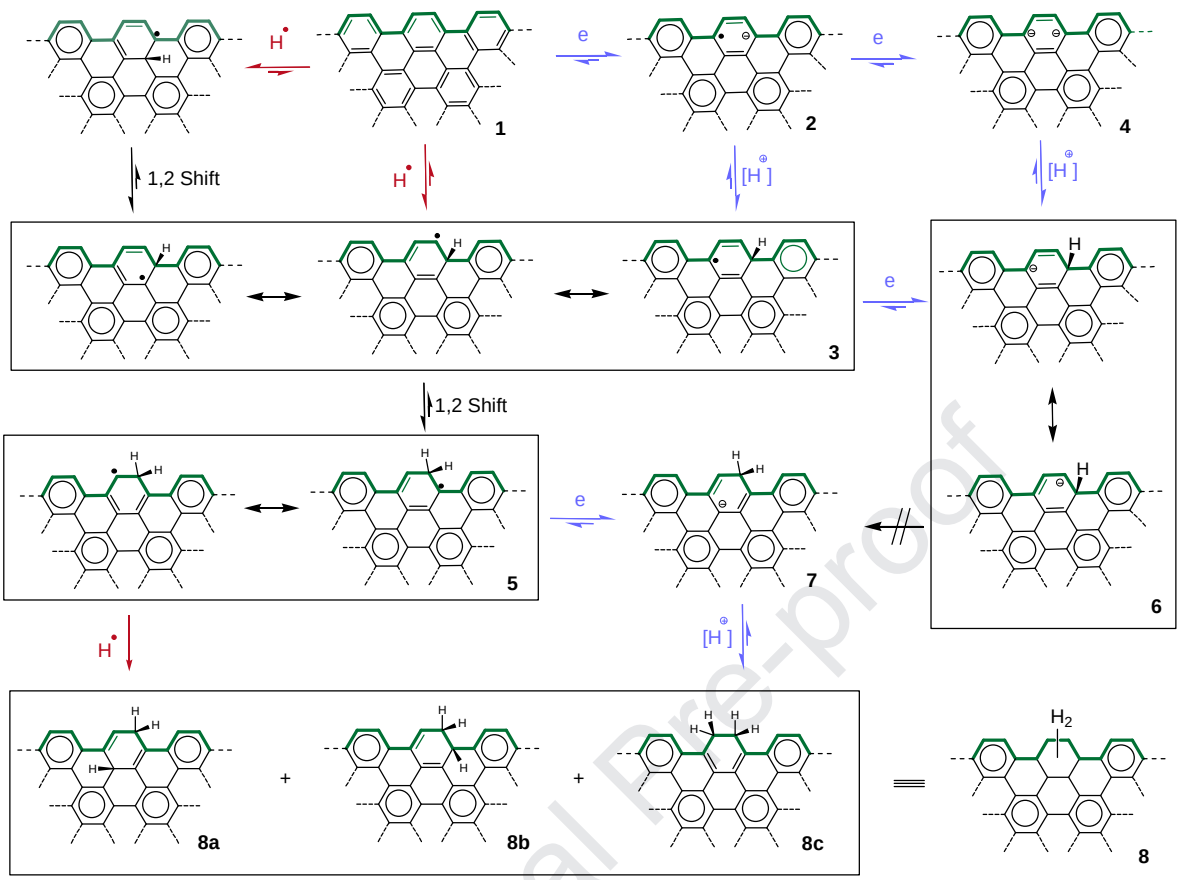

Scheme 1. Schematic representation of the mechanism of Birch-type graphene hydrogenation starting on the periphery (the periphery is highlighted in green). The mechanism of reductive hydrogenation (highlighted in blue) and of the mechanism direct radical hydrogenation (highlighted in red) show that the stabilities of intermediate radical species play a major role in the regioselectivity of both process.

2.3. Reductive graphene alkylation

The reductive alkylation is a related to the Birch hydrogenation, where the formed anion is trapped by a suitable electrophile such as alkyliodide, instead of the protonation by a proton donor. The Birch-type alkylation of simple aromatics is well studied process, [46, 47] whereas the alkylation of PAHs remains poorly explored. In our previous work, using hexabenzocoronene (HBC) as a model system for graphene we were able to gain insight into the complex mechanism of a single alkylation of reductively activated nanographenes.[42] It was found, that the first step consisting of a single electron transfer to alkyliodide leads to the fast formation of the alkylated HBC radical. This radical, however, cannot be stabilized by covalent bonding to the basal plane of nanographene and remains in the form of a van-der-Waals complex with a virtually isoenergetic hypersurface. In accordance with DFT

calculations the same behavior is expected for the graphene surface. [42] As a second step the alkyl radical can undergo a free movement over the basal HBC plane until a “defect” position at the edge will be found, where irreversible covalent binding to the graphene scaffold takes place. [42] This process is schematically summarized in **Scheme 2**. Similar to the hydrogenation the stability of the respective radical intermediates (9, 10 and 11) appears to be a key element in the alkylation mechanism, which predefines the final addition pattern. Moreover, the alkylation of the reductively activated graphene as well as a direct radical functionalization are both expected to lead to the same addition pattern, since the anionic character in the case of a Birch-type process is expected to play a minor role in the regioselectivity. This model is in a good agreement with experimental data showing that the functionalization proceeds from the perimeter to the interior of the graphene flake for both Birch-type hydrogenation,[35] and direct radical methylation.[48]

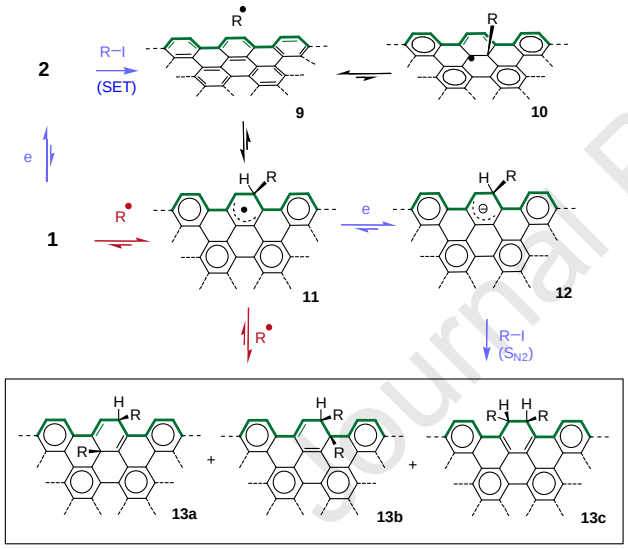

Scheme 2. Schematic representation of the mechanism of a reductive graphene alkylation (highlighted in blue) and the mechanism of direct radical alkylation (highlighted in red) showing that the stabilities of intermediate radical species play a major role in the regioselectivity of the process. The periphery is highlighted in green.

2.4. Multiple additions to the edges of graphene

The key principles of multiple additions to graphene can be derived by consideration of the regioselectivity of Birch-type reductions of small PAHs such as naphthalene (**16**) and anthracene (**14**) (**Scheme 3**).[49] Namely, the second dihydrogenation preferably takes place at the non-aromatic hexagon (partially hydrogenated benzene fragment) formed after initial 1,2- or 1,4- dihydrogenations (compounds **15**, **17** and **18**). Similar behaviour is observed for chrysene, pyrene, triphenylene and

other related PAHs.[46] The regioselectivity can be rationalized in terms of thermodynamic control leading to the formation of thermodynamically more stable products containing the largest possible number of Clar's sextets (**Scheme 3**). Note that the complete exhaustive hexahydrogenation of one benzene ring in the graphene lattice formally causes restoration of the original all-benzoid character. Therefore, the reactivity and the selectivity of subsequent hydrogenations should obey the same rule as it was discussed for starting situation. Reductive alkylations are expected to obey the same rules. Note, that due to steric hindrance the exhaustive alkylation of one benzene ring could be complicated in the case of bulky substituents. This however, as it will be shown later, has minor impact on the following addition sequences. We therefore propose that in a first approximation, the successive all-trans hexa-additions to aromatic sextets near the periphery or a pre-existing basal plane defect are predominant processes. Intuitively it is obvious that such a cascaded growth scenario ultimately leads to the progressive expansion of functionalized regions from the periphery to the interior of graphene flake and prevails over a homogenous addition to the graphene planes. This assumption is strongly supported by experimental observations considering the functionalization of graphene edges.[35],[48] It is worth mentioning, that among the stable arm-chair periphery the real graphene sheet contains the more reactive edges such as zig-zag. The last one, however, expected to react very fast yielding the all-benzoid π-system, which is expected to be similar in properties as arm-chair periphery flakes. Since the zig-zag periphery (after chemical etching) is expected to have no influence on the addition pattern, in this study we will consider only arm-chair peripheries. The "etching" process of zig-zag edges (structure **19**) leading to the quasi arm-chair periphery (structure **20**) is schematically shown in **Scheme 3d**.

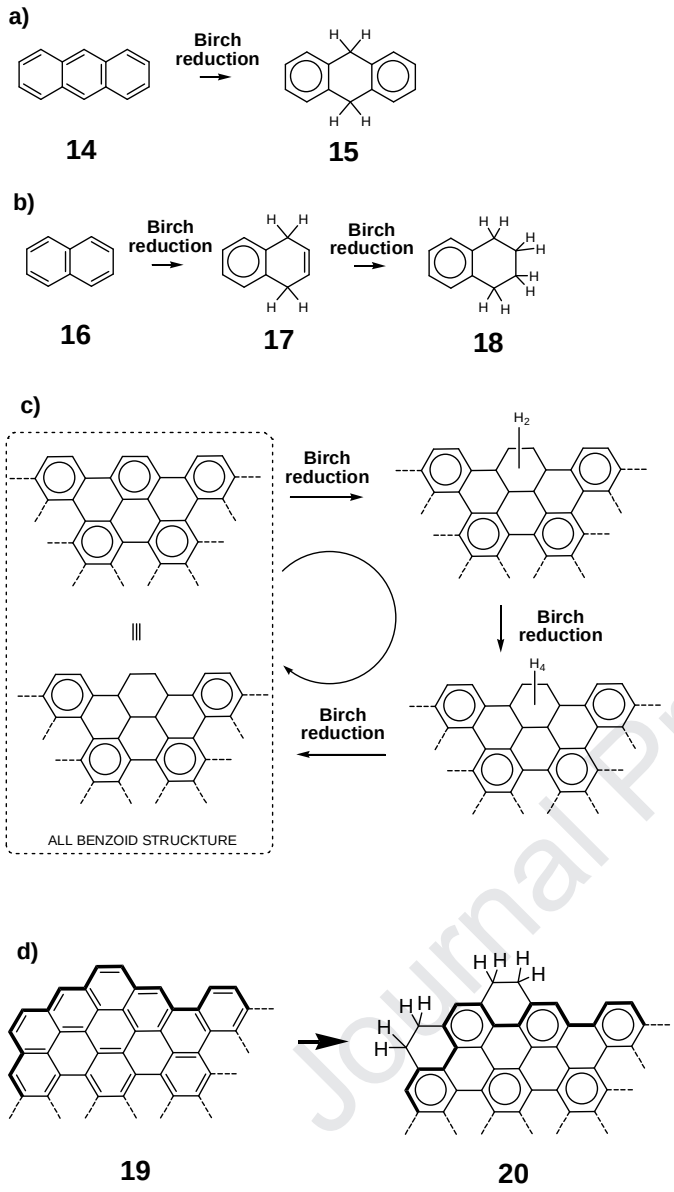

Scheme 3. Birch reduction of PAHs. a) Birch reduction of anthracene showing the preferable formation of all-benzoid 9,10-dihydroanthracene. b) multiple reduction of naphthalene showing the selective hydrogenation of double and inertness of the aromatic part c) schematic representation of the expected multiple reduction of the graphene periphery leading to the formation of all-benzoid product with maximum number of Clar's sextets. d) schematic representation of the etching of the zig-zag periphery leading to the quasi arm-chair periphery.

2.5. Addition to the basal plane of graphene

Theoretical predictions show that the direct addition to the ideal basal plane of infinite graphene surface is rather difficult. However, an effective functionalization of graphene has been demonstrated experimentally.[13-19] This can be connected with the fact that real graphene sheets are finite and

contain defects. In this work we show that imperfection in graphene lattice leads to the sufficient "activation" of the surface for addition. In this study, all possible structural imperfections within the graphene lattice including vacancies, holes, Stone-Wales defect, dislocations and sp^3 hybridized carbon atoms,[50] are referred to as defects. The introduction of any defect into the graphene lattice, including covalent attachment of a single H-atom,[51] inevitably leads to the perturbation of the π-electron system near the defect.[52, 53]

Such a perturbation is accompanied by distinct Clar sextet pattern formation as it is schematically depicted in **Figure 1**. It is important to point out that the same behaviour is observed at the periphery of the finite-size graphenes and nanographenes, where terminal hydrogen atoms can be treated as imperfections or defects (Figure 1c). From the chemical point of view, the most important conclusion is that the chemistry of the defected graphene surface can be described in analogy to the influence of edge defects at the graphene periphery discussed above and/or using small all-benzoid molecular models such as hexabenzocoronene (HBC) (**Figure 1d**).

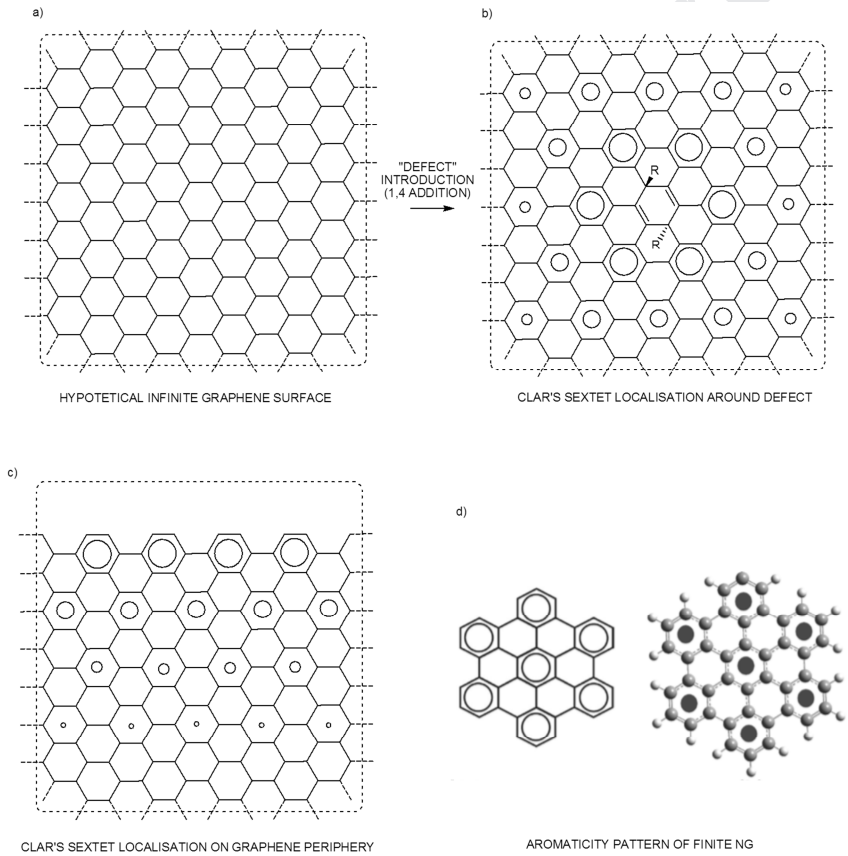

Figure 1. Schematic representation of defined Clar-sextet patterns in graphene/NG systems. a) infinite graphene surface with equally distributed π-density; b) re-organisation of the π-system and formation of aromatic Clar's

sextets around a defect. The size of cycles schematically indicates the degree of aromaticity; c) Aromatic Clar sextets along arm-chair periphery of graphene flake, the degree of aromaticity schematically indicated by the circle size; d) Clar aromatic sextet formula of hexabenzocoronene and the corresponding NICS aromaticity pattern (NICS map) which is fully consistent with Clar's theory. The size of cycles indicate the degree of aromaticity of individual hexagons (NICS(1) values adopted from 43)

Although the probability of direct functionalization of an "ideal" graphene surface is rather low we do not exclude this possibility. Moreover, despite the fact that such events are expected to be rare they could play a crucial role in the final distribution. An addition to the graphene scaffold leads to rehybridization from sp^2 to sp^3, which can be regarded as defect insertion activating the surface for further modification. This will cause a snowball effect leading to the consecutive defect expansion during functionalization. Based on basic reactivity considerations such as introduction or release if stain and conjugation energy we propose that additions to intact basal plane C-atoms are much less preferred than additions close to defects. It can be assumed that the probability of the direct functionalization in large and free-defect regions is negligible. As a consequence, the reactivity of defect-free graphene obtained from highly crystalline natural graphite is extremely low, since the "concentration" of in plane defects is close to zero. Once an in plane defect has formed the respective region will behave as a "defected" surface leading to the defect expansion as pointed out above. Putting this in other words: it is not necessary to distinguish between these cases since the reaction of both an "ideal" and a "defected" graphene surface will result in the same outcome in the terms of addition pattern. Moreover, as it will be shown below the initial concentration" of defect "seems to play minor role with respect to the addition pattern selectivity. Progressive addition steps will cause a continuous expansion of sp^3–regions rather than formation of new isolated defects. The expansion process is facilitated by the generation of the thermodynamically most favorable substructure motifs and leads to the formation of graphane-like islands (exhaustive or highly hydrogenated/alkylated graphene) incorporated into sp^2-carbon lattice of intact nano-graphenes. The global thermodynamic minimum is expected to be a mosaic-like 2D-carbon sheet containing graphane and intact graphene regions with the shortest possible border between them. However, if also kinetic factors come into play the final patterning could be drastically influenced. To address this important question, we have analysed and quantitatively described multiple radical attachments to the edges and the basal plane near defects/periphery with quantum mechanical calculations. Both thermodynamic and kinetic aspects

were considered. The radical attachments of hydrogen and methyl radicals were chosen as model reactions.

2.6. Single hydrogen radical addition

The covalent binding of single hydrogen atoms to defect-free graphene surface has been intensively investigated using periodic *ab initio* calculations. [54-58] However, the approaches applied previously lead to rather different results due to the sensitivity to the computational method applied. According to previous DFT calculations the energy of hydrogen radical addition to graphene vary in the range between 12 and 22 kcal/mol.[54-58] These mismatches are mainly associated by the use of oversimplified approaches instead of involving more accurate hybrid exchange-correction functionals. Moreover, representing the infinite graphene crystal as a periodical cell with insufficient size does not allow to estimate energies accurately, because the addition to the graphene lattice induce a large-area distortion of the sheet.[59] For the same reason the estimation of the binding energy using finite nanographenes as a model appears to be difficult. Thus, in ref. [59] the authors point out that the accurate value of chemisorption energy cannot be obtained from the finite cluster model showing that for nanographenes of various size ($C_{13}H_9$, $C_{37}H_{15}$, $C_{73}H_{21}$, $C_{121}H_{27}$ and $C_{181}H_{33}$) the DFT derived binding energies oscillate in a wide range (from ~14 to ~37 kcal/mol). The authors conclude that the energy oscillation is caused by the finite cluster approach itself, rather than by the level of theory and the systems with less than 200 carbon atoms are not sufficiently large enough to provide the convergence. However, the nanographene model used in this work represents an open-shell system and thus cannot be considered as representative model for the graphene surface. Considering nanographenes as graphene models the aromaticity pattern, which plays a major role in the PAH reactivity, has to be taken into consideration. In this respect the so-called all-benzoid PAHs with pronounced benzenoid character, very reminiscent the graphene aromaticity, appear to be the most suitable model systems.[60] Indeed, the estimation of binding energies for close-shell PAH systems on B3LYP level of theory gave reasonable values in the range of 15-20 kcal/mol,[61] which is in good agreement with periodic calculations. Moreover, B3LYP and PBE level of theory, both were found to be accurate enough for the investigation of the hydrogen chemisorption process showing good agreement with a rigorous benchmark CCSD level of theory calculations,[62] which has become established as the “gold standard” in modern quantum chemistry.[63]

Our calculations for the single hydrogen radical chemisorption to the pristine graphene surface utilizing periodic PBE approach and relatively large 12×12 unit cell gave value of 19.8 kcal/mol. Estimation of the energy binding on B3LYP/def2-SVP level using all-benzoid HBC ($C_{42}H_{18}$) as a nanographene model resulted in essentially the same value of 20.4 kcal/mol). The activation barrier of hydrogen attachment was found to be close to 5.0 kcal/mol (25 kcal/mol for detachment process respectively) which is in good agreement with previously reported data, (4.6-5.1 kcal/mol),[55, 64, 65] including CCSD level of theory.[62] Thus, both approaches used in this study (periodic PBE and molecular B3LYP) appear to be accurate enough for the investigation of graphene chemistry. Furthermore, as it was discussed above, the addition preferably takes place close to the graphene periphery or defects. Thus, the use of finite molecular models seems to be an even more accurate approach for describing the chemistry of the "real" graphene and related systems.

2.7. Thermodynamics of the multiple hydrogen addition

Assuming that H-shifts can easily take place the formation of the thermodynamically most favorable addition pattern could be expected. To analyse this possible scenario, we have performed a thermochemical analysis of multiple graphene hydrogenations involving a periodic PBE approach using a relatively large (12×12) unit cell. For this purpose, we have evaluated the reaction enthalpy for each individual dihydrogenation and compared these relative values. The consideration of the model reaction $C_n+H_2 \rightarrow C_nH_2 + \Delta H$ consisting in the formal addition of molecular hydrogen (H_2) to graphene (C_n) provides energy values (enthalpies ΔH). These values are expected to correlate with the free Gibbs energy assuming the same entropy contribution for each addition. Note, the relative enthalpies ($\Delta\Delta H$) are independent on the reaction mechanism and can be applied for the analysis of alternative hydrogenation reactions (e.g. additions of hydrogen radicals).

Considering the thermodynamics of the formal H_2 addition to the basal plane we have found that 1,2-*anti* addition is the most favourable process. All alternative patterns including 1,4-*anti*/*syn,* 1,6-*anti/syn* and 1,2-*syn* lead to the energetically less favourable geometries. The 1,3-*anti*/*syn and* 1,5-*anti/syn* were found to be highly unfavourable due to open shell character of the respective adduct. The 1,2-*syn* addition was found to be 12,3 kcal/mol higher in energy that the respective *anti*- addition which corresponds to about 6,2 kcal/mol per each C-H bond (**Figure 2**). Interestingly, further *syn*-additions do not provide effective relaxation of the system. Thus the difference for all-cis addition of

six hydrogen atoms the difference increases further to 7,2 kcal/mol per C-H bond (42,9 kcal/mol, **Figure 2**). In our model we have analysed only consecutive *anti*-1,2 hydrogen additions since all alternative additions were found to be less favourable.

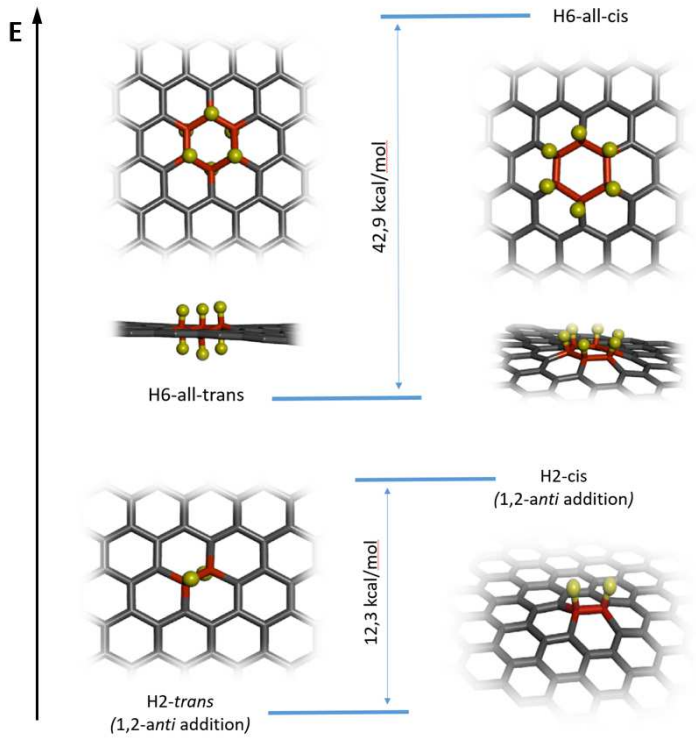

Figure 2. Optimised geometries and relative energies of 1,2-syn- and 1,2-anti- addition pattern on the example of perhydroethylene-hole and perhydrobenzene-hole formation.

For each subsequent addition the preceding hydrogenation pattern was considered to be static (no further hydrogen rearrangement was considered for the pre-existing H-pattern). The detailed analysis of possible hydrogenation patterns allowed us to evaluate the thermodynamically most favorable pathway, which is summarized in **Figure 3**.

Pristine graphene (**21**) provides only one possibility for an *anti*-1,2 addition (structure **22**), since all C-C bonds in **21** are equivalent. This addition represents an endothermic process and requires 27.0 kcal/mol which can be understood in term of local de-aromatization reducing the total number of Clar's sextets by one. In addition some local strain energy that is introduced to the adjacent local sp^2-network, which is now slightly deviating from planarity. The perturbation of the "ideal" graphene π-system leads to the reorganisation of the electron densities around the incorporated "defect". Thus, for

the second addition many non-equivalent positions are offered. However, our PBE analysis shows that only eight double bonds close to the "defect" are "activated" for the next reaction. The activity rapidly decreases with increasing distance from the defect, quickly approaching the enthalpy of H_2- addition to the defect-free graphene. From a thermodynamic point of view, the perturbed graphene region appears to be rather small, which is schematically shown in **Figure 3** by circles with radii of about 5Å. All additions outside the circle are virtually equal in energy to the addition to the pristine graphene (see SI). All respective symmetry non-equivalent positions are coded by different colors. The structure **22** has only two symmetry non-equivalent sites "activated" for the hydrogenation, leading either to **25** or to **24**, requiring only 4.4 or 8.3 kcal/mol respectively. Note, that despite the close proximity to the defect one of the positions in **22** is highly deactivated (coded in blue) in comparison to the pristine graphene (27.0 kcal/mol). This addition would require unrealistic 42.4 kcal/mol which can be explained by the formation of an extended quinoide motive (structure **26**) drastically reducing the number of Clar's sextets. It is worth to mention that considering the hydrogenation as 1,2 addition process solely, does not mean that possible 1,4 additions is ignored in the model. Indeed, the most stable configuration for terahydrogenated graphene (**25**) can be imagined as a 1,4 addition to **22**. Since in the thermochemical analysis the detailed addition sequence does not play a role both processes provide the same enthalpies and thus can be correctly described using only consecutive 1,2 additions. Thus, for example the less favorable (but still possible) 1,4 addition to **21** (structure **23**) will be followed by 1,2-hydrogenation yielding the same the most stable configuration **25**. The second 1,4 addition to **23** would lead to **26** which can be considered as a highly unrealistic event.

For the third bis-hydrogenation three alternative ways leading to **27**, **28** and **29**, respectively, can be considered. The most probable scenario is the formation of **28** which is already an exothermic process (-9.7 kcal/mol). Such an energy gain can be rationalized by the formation of a "perhydro benzene hole" (PH-benzene-hole) incorporated into a graphene lattice. The remaining π-structure **28** can be considered as an all-benzoid system with the maximum number of Clar's sextets. Because of the high symmetry of **28**, only one possibility for the next addition is offered (12 symmetry-equivalent positions), which is a "perhydrostyrene hole" (PH-styrene-hole, structure **30**). Very importantly, the fourth bis-hydrogenation of the alternative products **24**, **27** and **29** will lead almost exclusively to the formation of the same PH-styrene-hole structure. Thus, the consideration of the most stable addition patterns appears to be sufficient and accurate for the prediction of the thermodynamically most

favourable hydrogenation pattern. As a consequence, despite the numerous alternatives for successive hydrogenations the main "expressway" leading to the most stable target geometries will finally be found. In the case considered here the most favorable hydrogenation route is highlighted by the red background in the **Figure 3**. Extrapolating these arguments shows that hydrogenation leads to the formation of stable motifs containing perhydro-PAH-holes (PH-PAH-holes) in the remaining graphene lattice. Further, the progressing hydrogentation of **30** lead to the formation of either perhydronaphthalene (PH-naphthalene-hole, **32**) or PH-biphenyl-hole (**31**) units. Note that both of them will finally lead to the formation of PH-phenanthrene-hole (**34**).

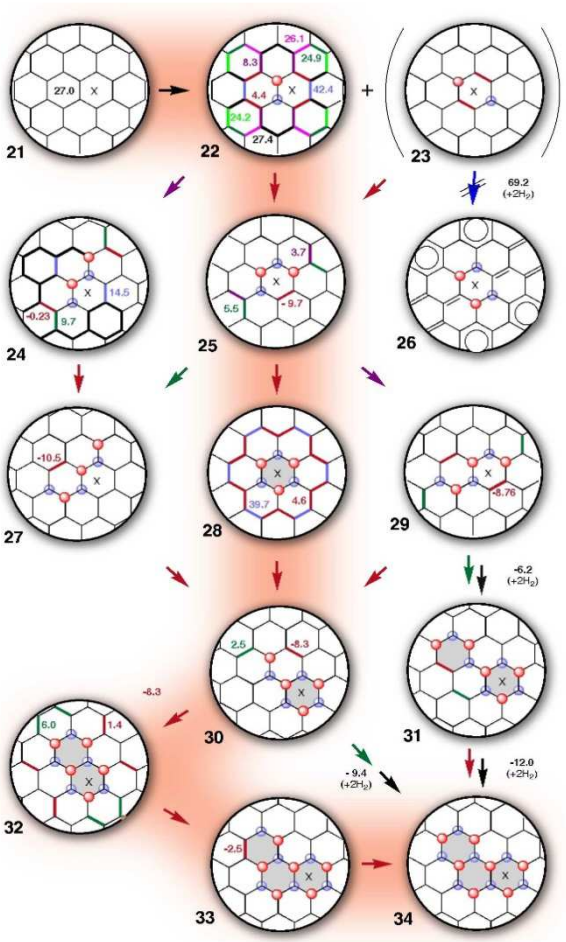

Figure 3. The evolution of the thermodynamically more favorable oligo-hydrogenation pattern. The most favorable path is highlighted by the red background. The top/bottom hydrogen attachment is indicated in red and blue respectively. The symmetry non-equivalent positions for hydrogenation and the respective enthalpies in kcal/mol are coded with the same colors. The energetically most favorable case is highlighted with red arrows. The color of arrows corresponds to the addition to the respectively coded C-C bonds. One of the hexagon is labeled with "X" as a guide for the eyes. The gray background indicates the formation of PAH-perhydro-holes.

Considering higher degrees of hydrogenation we found that the incorporation of PH-PAH-holes always leads to the energetically most favorable solutions. The formation of hydrogenated chain-holes, for example, is energetically less favorable. As it can be seen from **Figure 3** the total enthalpy continuously decreases during expansion of the PH-hole defect, approaching the value of graphane (-7,84 kcal/mol calculated per one CH group). After addition of 8-9 H_2 molecules the enthalpy of addition becomes negative. Interestingly, the relative stability of the hydrogenated graphene system with incorporated PH-PAH-holes correlates with the stability of the parent PAHs. Thus, the introduction of a PH-phenanthrene-hole unit is more favorable than the introduction of PH-anthracene-hole. The introduction of a PH-tetracene-hole requires more energy than the introduction of a PH-tetraphene- or PH-chrysene-hole. However, this differentiation tends to decrease with an increasing degree of hydrogenation indicating that the expansion of the large PH-PAH defect is expected to be virtually isoenergetic in all directions (e.g. three different PH-PAH-holes formed by addition of 22 hydrogen atoms provide virtually isoenergetic structures, **Figure 4**).

Summing up, the hydrogenation of graphene can be easily rationalised on the basis of Clar's concept of aromaticity and can be considered as a three step process:

(i) defect nucleation. The direct hydrogenation of a defect-free graphene surface is expected to be a very rare event. However, addition can easily take place close to the pre-existing or fluctuationally generated defect leading to the removal of one Clar's sextet and the generation reactive double bonds in the same six-membered ring

(ii) strain relaxation. After defect nucleation the subsequent hydrogenations proceed easily, leading to rapid relaxation *via* exhaustive functionalization of the initially "defected" hexagon. The final structure (in close proximity to the formed PH-benzene hole) is characterized by pronounced all-benzoid character of the remaining π-systen. Further reduction of strain energy takes place *via* selective formation of stable PH-PAH-holes (PH-benzene-hole -> PH-naphthalene-hole/PH-biphenyl-hole ->PH-phenathrene-hole -> PH-pyrene-hole/PH-triphenylene-hole). This process leads to efficient strain release caused by the mismatch of the graphene/graphane lattices. Note, the preferable formation of PH-PAH-holes displaying connectivity of "all-benzoid" PAHs is a direct consequence of the formation of stable π-system exhibiting the maximal possible number of Clar's sextets.

(iii) defect expansion. After addition of 14-18 hydrogen atoms the hydrogenation is expected to proceed smoothly on adjacent hexagons with a similar probability in all directions leading to a variety of differently shaped “all-benzoid” PH-PAH-holes asymptotically reaching the energy of graphane.

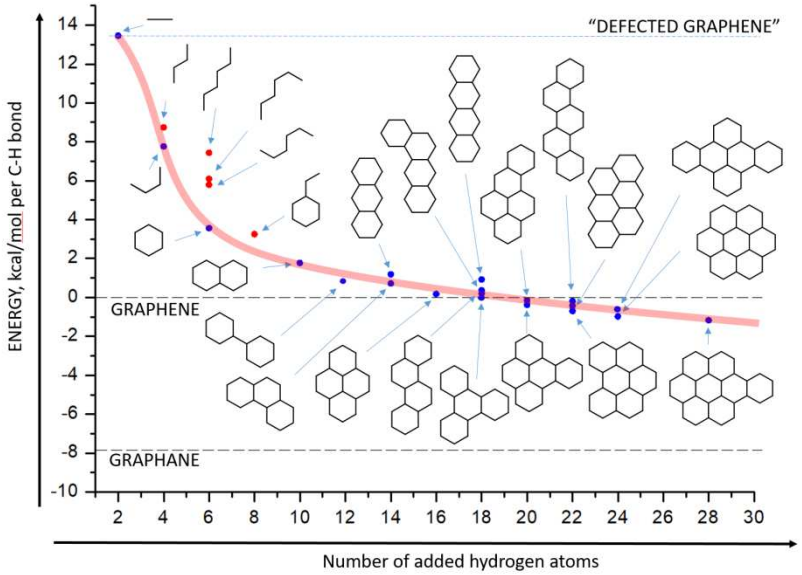

Figure 4. Reaction profile of the hydrogenation of graphene. The relative energies are given for several selected thermodynamically most stable structures containing PH-PAH-holes. The line “defected graphene” (perhydroethylene-hole) corresponds to the approximate starting points in the case of the addition to the pre-existing defect.

2.8. Kinetic consideration of the multiple hydrogen addition

Quantum chemical calculations show that the addition of a single hydrogen radical to the periphery of nanographene has a remarkably lower activation barrier compared with an addition to the basal plane. However, the question how this addition would influence subsequent hydrogenations was not addressed in the literature. To investigate this process, we have analysed the activation barriers of hydrogen radical addition to partially reduced HBC as a nanographene model. Note, all partially hydrogenated HBC molecules have an all-benzoid character (minimizing the contribution of additional electronic factors on the obtained activation energy values).

The barrier of hydrogen addition to the central ring of HBC was found to be 4.51 kcal/mol which is rather close to the activation barrier for hydrogen addition to the basal plane of graphene (~5,0 kcal/mol) despite the rather short distance to the edge (**Figure 5**). This additionally indicates that the perturbation area is very small and the activity in the addition is only expected for carbon atoms placed

close to the periphery. Note, the same behavior was also predicted from the thermochemical analysis. The incorporation of one PH-benzene-hole into HBC leads to significant reduction of the activation barrier to 0.6 kcal/mol (**Figure 5**). Interestingly, that the introduction of second and third PH-benzene-hole results in a slight increase of the activation energy to 1,0 and 1,3 kcal/mol respectively. Such a behavior can be understood considering the cumulative effect of the electronic and steric factors on the stability of the respective radical species. Thus, the product of radical addition to the center of the pristine HBC can be effectively stabilized due to delocalization of the radical center between three positions as it is shown in **Figure 5**. Each respective resonance structure remarkably contributes to the overall stability due to its benzylic character. However, the incorporation of sp^3 hybridized carbon into planar sp^2 lattice requires a highly unfavorable geometry which is accomplished by the strain energy increase. Note, that all alternative resonance structures with delocalization of the radical center over lager regions provide minor contributions to the overall stability because of their quinoid nature. The addition to the HBC with one PH-benzene-hole provides the same opportunity for radical delocalization (three benzylic positions). However, the strain energy is much less since one of the neighboring carbon has sp^3 hybridization. Addition to HBC with two and three PH-benzene-holes provides even more suitable (less strained) geometries, however the electronic stabilization, with two and one benzylic positions correspondingly, is less effective. Slight increases in the activation energy indicate that the electronic effect has higher absolute value which is in line with results obtained from thermochemical analysis demonstrating that the strain can be effectively released by “incorporation” of just few additional sp^3 carbon atoms close to the defect.

It is important to mention that the differences of 3-4 kcal/mol in the activation energies are sufficient to expect a notable selectivity for subsequent binding steps. Thus, the estimation of the relative rates using Arrhenius equation shows that the addition to the PH-benzene-hole-HBC is about 800 times faster than the addition to the parent HBC. Taking into account that the hydrogenation is typically carried out at low temperatures a high regioselectivity is expected (**Figure 5**). Thus for instance, by carrying out the hydrogenation under standard dry-ice bath temperature (~ -78^{o}C) the difference will reach the value of $24x10^3$ times.

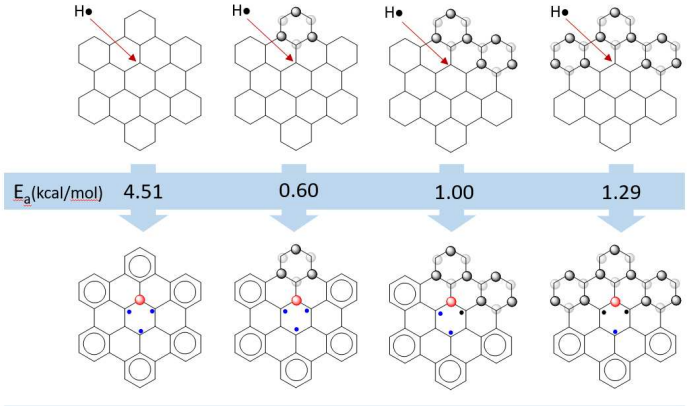

T, °C	RELATIVE REACTION RATES k_1/k_2			
20	1	830	420	250
0	1	1350	650	380
-33	1	3650	1580	860
-78	1	24240	8630	4080

Figure 5. DFT-derived activation energy for hydrogen radical addition to HBC-based models.

2.9. Alkylation of graphene

Considering the addition of alkyl radicals to the basal plane and addition close to defects reveals that the regioselectivity of the addition is qualitatively the same as those discussed for the hydrogenation. Similarly to hydrogen radical (which migrates over the surface *via* 1,2-H-shifts) the alkyl radical can freely migrate over the π-surface of graphene. The non-covalent character of C-C binding of alkyl radicals to the basal plane has been predicted theoretically.[66] Thus for example the barrier of methyl radical addition was found to be only 10 kcal/mol and about 15 kcal/mol for the back reaction.[42] In comparison the barrier for covalent attachment of hydrogen radical is close to 5 kcal/mol whereas the detachment process is characterised by the rather high barrier of about 25 kcal/mol.[67] According these data, the traveling of the alkyl radical species over the graphene surface, should result in the effective migration of radicals close to the pre-existing defects (or edges) where radicals can be stabilized *via* covalent addition. Recently, this assumption was confirmed experimentally on model HBC-based nanographene system.[42]

Since the mechanism proposed in this study provides a very good guideline to predict the regioselectivity of multiple radical additions, the important question of structure patterning of chemically functionalized graphene can be addressed. It is important to underline, that both thermodynamic and kinetic considerations arrive at the same conclusion, namely, an effective activation of the π-system for additions is expected only in close proximity to a pre-existing defect.

From a thermodynamic point of view, the expansion of larger PH-substructure-holes is more or less isoenergetic in all directions with a slight preference to form disc-like PH-PAH-holes. Kinetic data also support preferred binding to sp^2-C-atoms in direct neighbourhood of defects. In the latter case, however the preference is shifted to the formation of branched dendrimer-like PH-PAH-holes. Since all positions close to the defect are activated and the differences between them are rather small (considering both thermodymamic and kinetic effect), effective addition is expected as soon the radical will reach one of these centers.

2.10. Monte-Carlo simulations

As it is shown above any imperfection in the graphene lattice leads to a defined patterning with Clar sextets close to the defect. This is in accordance to a recent theoretical study on graphene aromaticity at boundaries and/or close to the defects. [41] In our model we suppose that the addition could take place exclusively close to defects. Therefore, the graphene lattice can be considered as an all-benzoid system with localized aromatic sextets, which is in full agreement with the empirical Clar theory and our kinetic and thermodynamic analysis of the graphene reactivity. (**Figure 6a**) As it is discussed above perturbation of the all-benzoid structure during functionalization will results in localisation of double bonds in the "defected" hexagon (**Figure 6a**) which greatly facilitates the formation of PH-benzene holes restoring the initial all-benzoid character (**Figure 6b** and **6c**). The introduction of such PH-PAH holes results in the activation of neighboring hexagons for the next addition (**Figure 6c, 6d**). Based on this model we have performed a set of numerical Monte-Carlo simulations of multiple additions to graphene assuming that intermediate radical adducts can move over the π-surface of graphene (**Figure 6d**) and undergo irreversible covalent binding as soon as the active site has been reached (a detailed description of the model is provided in the SI). After this event the fast addition to the double bonds is expected which leads to the (as example) PH-biphenylene-hole formation (**Figure 6e**). Worth to mention that if the exhaustive functionalization of "defected" Clar sextet was not completely achieved this will not influence the following addition scenario since the number of addends does not influence the Clar pattern (**Figure 6a, 6b and 6c**). Thus, in the model the event of radical attachment to the active sites is attributed to the complete functionalization of the respective hexagon (formation of the PH-biphenyl-hole). As it is shown in **Figure 6e** the formation of the PH-biphenylene-hole increases the number of active sites to eight. The next addition could lead

either to a PH-triphenylene-hole (**Figure 6f**) or a PH-terphenyl-hole (not shown). Thus, the graphene surface can be considered as a triangular lattice where each site corresponds to the Clar sextet (**Figure 6g, 6h, 6i**). In our simulations we place the radical on the randomly selected site which undergoes random jump to the neighboring positions until the active site will be found. On this point the radical either undergos addition to the site according to the predefined in model addition probability factor (depending on the microstructure of surrounding) or continues to migrate further. This addition event corresponds to the to the exhaustive functionalization of the respective hexagon (removal of one Clar sextet) which is accompanied by the activation of all neighboring sites as it shown in the **Figure 6**. All simulations were performed for the lattice with periodic boundary conditions with up to 138400 Clar sextets which corresponds to the 830400 carbon atoms in the cell.

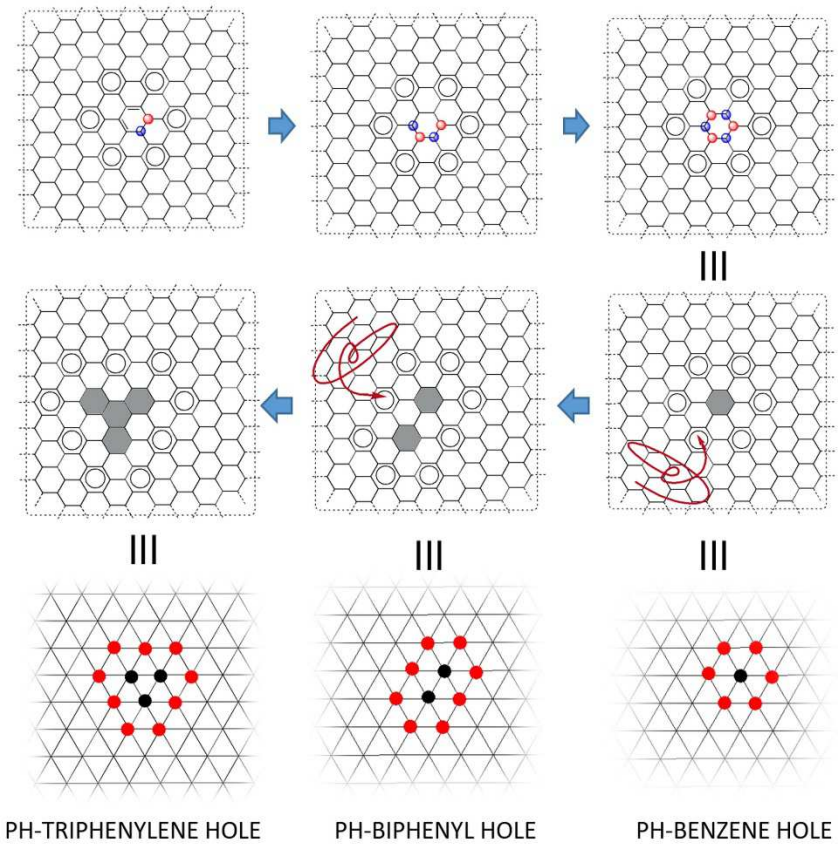

Figure 6. Schematic representation of the model. a) b) c) formation of PH-benzene-hole leading to the active sites generation around the hole d) e) f) schematic representation of the radical traveling to the active sites, active for addition Clar sextets are highlighted in red; g),h),i) representation in the triangular lattice, red circles indicate active for addition sites (active Clar sextets), black circles indicate PH-benzene-holes.

The possibility to differentiate the relative site activity depending on the surrounding microstructure (number of PH-benzenes in the close proximity) allows to simulate and analyse the influence of both kinetic and thermodynamic factors on the functionalization pattern. It has to be kept in mind that the migration ability of radicals could have notable impact on the overall regioselectivity and therefore the final addition pattern. If the radical can easily migrate over the graphene surface, more pronounced regioselectivity can be expected. In contrast, if the radical migration is restricted or hindered, the covalent bond formation between the attacking radical and a basal plane C-atom will take place on the first approached active center. Since the migration ability is influenced by many factors including temperature, solvent, addends, counterion nature and the radical stability, it is not possible to estimate all those contributions quantitatively. However, this parameter can be analysed with the presented model and the mobility effect can be qualitatively extracted. This will now be demonstrated with four selected boundary model scenarios **A-D** which are summarized in table 1. In the model **A,** the addition always takes place as soon a radical reaches one of active site (attachment probability g_{fix} = 1). In model **B** the probability of attachment is set to 10% (g_{fix} = 0.1). This model simulates a higher mobility of the radical since the radical can "visit" several possible centers before addition. The model **C** qualitatively simulates the thermodynamic contribution (thermodynamic control) where the probability of the addition increases with the increase of number of "defected" sites in close proximity (**Figure 7**). In contrast model **D** simulates a kinetically controlled process where the most favorable addition is expected for sites adjacent to only one PH-benzene-hole (**Figure 7**). All four models were used for the simulation of multiple addition to graphene starting from (i) a graphene layer with a single defect in the basal plane, (ii) graphene layers containing several defects (0.01% and 0.001% of defects) and (iii) the edge functionalization of a defect free graphene flake.

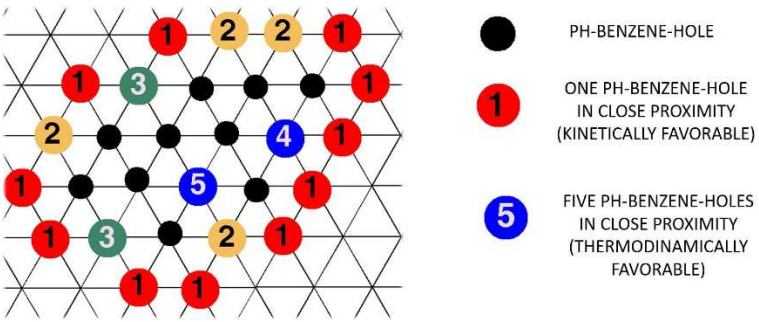

Figure 7. Sites activity differentiation depending on the number of neighbouring PH-benzene-holes.

Table 1. Relative probabilities (g_{fix}) of addition to active sites depending on the number of PH-benzene holes in close proximity**.**

Model	Number of neighboring PH-benzene-holes					
	0	1	2	3	4	5
Model A	0	1	1	1	1	1
Model B	0	0.1	0.1	0.1	0.1	0.1
Model C	0	0.1	0.2	0.3	0.4	0.5
Model D	0	0.5	0.4	0.3	0.2	0.1

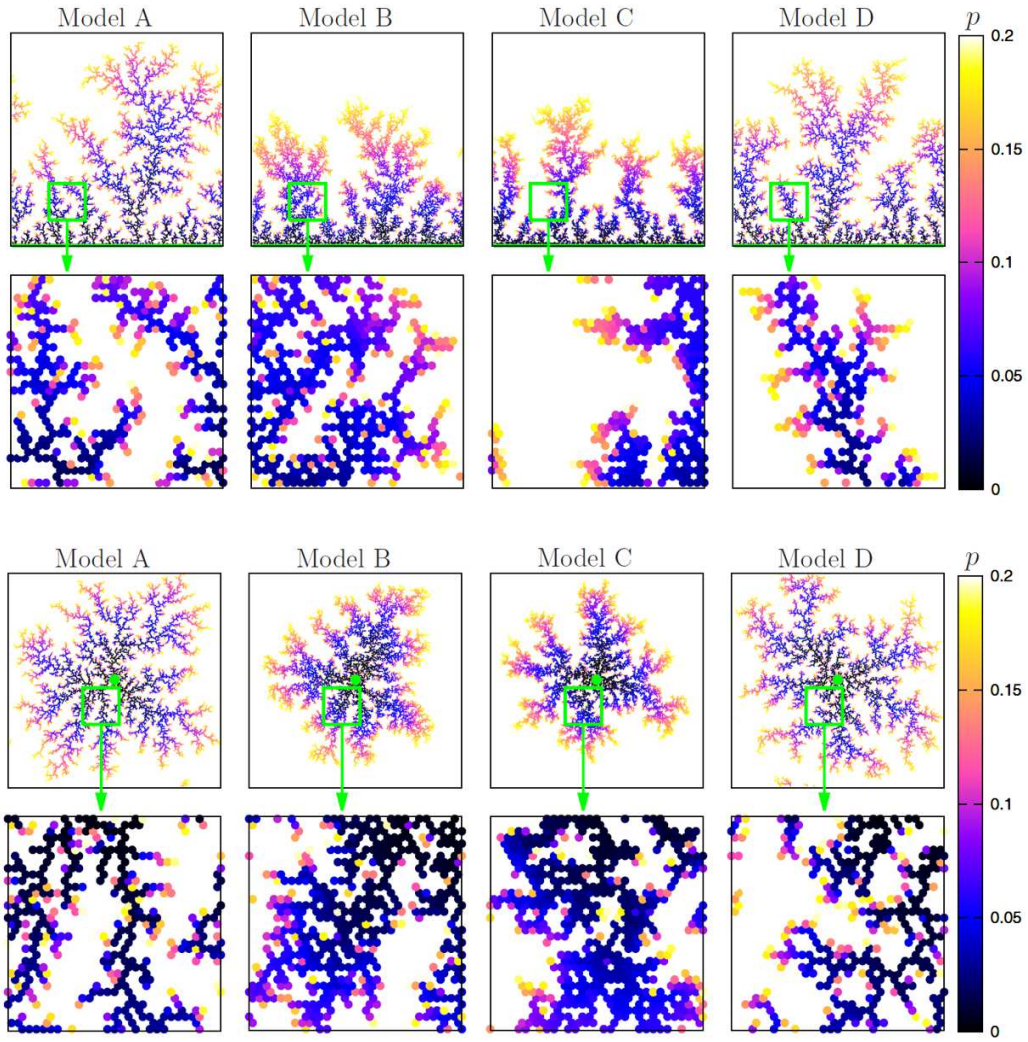

Figure 8. Graphical representation of the DLA-like defect expansion on graphene: (a) defect expansion on graphene edges. (b) defect expansion on the basal plane starting from single defect. The starting point is highlighted with a green point. The microstructure of an addition-pattern is shown in the inserts, indicating denser PH-PAH-hole formation for model **B** and **C**. The color of the element (p) represents the "time" of addition.

.

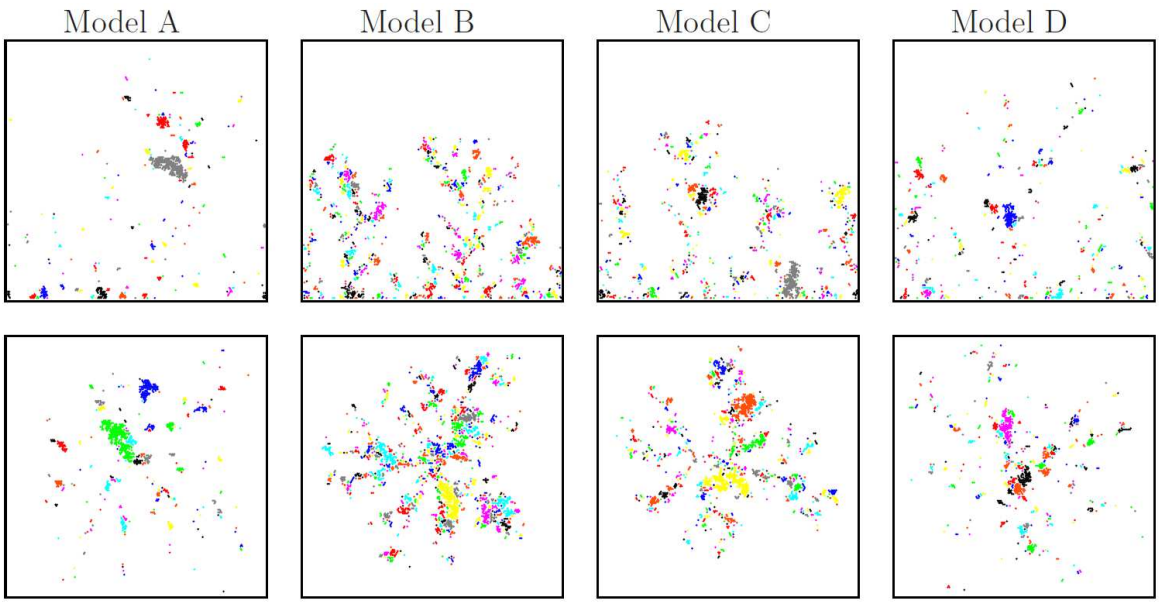

Figure 9. Graphical representation of the aromatic island formation during DLA-like defect expansion on graphene for models A-D. Top row for the expansion from the periphery (corresponds to structures shown in **Figure 8a**). Bottom row – for the defect expansion from the single defect (corresponds to structures shown in **Figure 8b**). Different clusters are indicated by different colors.

It was found that independent of the model used the simulations reveal rather similar growth patterns, which can be defined as a "diffusion-limited aggregation" (DLA) (**Figure 8**). This process is widely spread in nature, both on the molecular level and for small particle.[68-71] Some cases of DLA are known under the name of Lichtenberg Figure, Brownian tree or Fractal-Seaweeds.[72, 73] Typical forms of these aggregates are irregular dendrimers closely related to fractals.[74] The analysis of the cluster size distribution as a function of degree of addition (PH-PAH-holes) shows that models **A** and **D** are characterized by less dense functionalization than model **B** and **C**. Independent of the model the DLA-like defect expansion leads in the formation of isolated aromatic islands (PAH fragments isolated by graphane) which is in a good agreement with the previously made assumption on the base of experimentally observed fluorescence of hydrogenated graphene in the solid state.[15] The aromatic island size distribution as well was found to be similar for model **A** and **D** showing small cluster formation, and model **B** and **C** which are characterized by the formation of more extended aromatic regions as it illustrated in **Figure 9** (For analysis of cluster distribution see SI). It is worth mentioning that it is difficult to distinguish the results obtained from models **A** (low mobility) and **D** (kinetic control) indicating that the low mobility of radicals and kinetic effects provide qualitatively equal

contribution in the context of functionalization pattern. Even more interesting the similarity between models **B** (high mobility) and **C** (thermodynamic control) showing that higher mobility of radicals direct the addition to the thermodynamically more favorable pattern. Putting in other words, the addition can be simulated by a single parameter g_{fix} (apparent reactivity), which includes the contribution of all additional factors (including kinetic, thermodynamic, mobility, temperature). Therefore, models **A** (g_{fix} = 1) an **B** (g_{fix} = 0.1) can be considered as two border causes. Taking into account the high reactivity of radical species (low activation energies for addition) we consider the model **A** as the most representative one. This assumption however has to be proven experimentally in future.

Further, we have analyzed the effect of concentration of preexisting defects on the addition pattern and found that the final microstructure is virtually unaffected by this factor. Thus, simulations with graphenes containing 0.001% and 0.01% of preexisting defects provide rather similar addition patterns. As a consequence, the influence of the concentration of pre-existing defects on the regioselectivity of addition appears to be negligible. These results show, that our model is very robust and general. Its applications are widespread including the description of Birch-like hydrogenation, reductive alkylation and direct radical addition independently on the size, shape and even quality of the graphene flakes.

Moreover, the expansion of defects starting from the periphery was analyzed in more detail. Since for large-size graphene flakes the probability of direct addition at the periphery is negligibly small (at least at the early stages of functionalization) the functionalization of the periphery is mainly a result of massive radical migration from the graphene surface. This scenario was simulated by the radical “deposition” on the top line of the graphene cell, whereas the evolution of defects was analyzed on the opposite side (for detail see SI). Treating the functionalization density as a function of distance and time we observed a rapid saturation of the concentration of addends in the range of 10 to 25% (depending on the model). After this point a further expansion of the defects with equal density of the functional groups, providing rather homogenous functionalization, was predicted (**Figure 10**). These results are in an excellent agreement with experimental data of photoinduced methylation of graphene, showing the progressive expansion of functional regions from the periphery with the relatively low degree of functionalization and constant degree of functionalization as indicated by Raman spectra showing constant intensity ratio of the D band to G band ($I_D \backslash I_G$).[48]

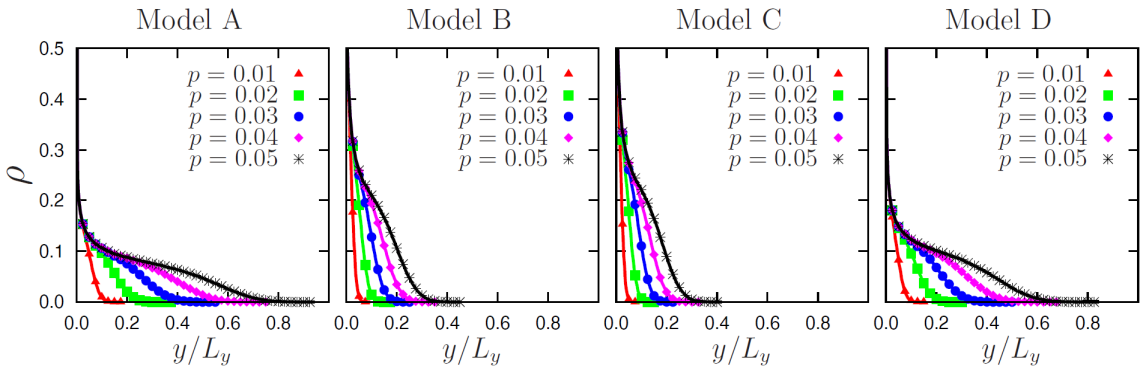

Figure 10. Simulation of the graphene edge functionalization showing functionalization density as a function of "time" p (fraction of added radicals) and distance from the edge.

3. Conclusions

Summing up, we have demonstrated that the regiochemistry of the reductive hydrogenation/alkylation of graphene can be rationalized as a radical addition process. Quantum chemical considerations of multiple radical additions to the graphene, reveal virtually the same selectivity in the addition for kinetically and thermodynamic controlled reactions. This allows us to develop a general model for multiple additions and to predict the complex addition pattern of reductively functionalized graphene. Based on the extensive quantum chemical calculations supported by the previously obtained experimental observations we show that addition to graphene takes place predominantly close to defects (or periphery) as all-*trans* addition. This process ultimately leads to the progressive expansion of the defected area *via* formation of all-*trans* PH-PAH fragments incorporated into the graphene matrix. It is shown that the selective formation of PH-PAH fragments is driven by keeping the all-benzoid character of remaining π-system which is in accordance with the Clar theory of aromaticity. Based on Monte-Carlo simulations we demonstrate for the first time that homogeneous functionalization of the graphene surface is highly unlikely process and the addition pattern can be rationalized as a DLA-like fractal defect expansion. This progressive expansion leads to the formation of fractal-seaweeds pattern explaining many unusual experimental observations, including the low degree of functionalization, formation of separated aromatic islands and the enhanced reactivity of edges. The presented model allows prediction and analysis of the structure of functionalized graphene including analysis of functionalization pattern, cluster distribution and the degree of functionalization. We show that kinetic and thermodynamic contributions and its influence on the addition can be analyzed quantitatively, which makes the model robust and applicable for describing of a wide scope

of reactions. Possible applications include the description of Birch-like hydrogenation, reductive alkylation and direct radical addition. Moreover, the model provides the possibility to estimate qualitatively the contribution of various factors (such as radical mobility, temperature as well as graphene flake size and quality) on micropattern evolution during addition. This makes the model a powerful and versatile instrument in the chemists' analytic toolbox. We truly believe that our finding will substantially contribute to the blooming field of graphene chemistry.

Supporting Information

Supporting Information (theoretically optimized coordinates, energies and model description) is available from the Wiley Online Library or from the author.

Acknowledgements

Funded by the Deutsche Forschungsgemeinschaft (DFG) – Projektnummer 182849149 – SFB 953). The work was supported by Act 211 Government of the Russian Federation, contract № 02.A03.21.0011

REFERENCES

[1] C. Lee, X. Wei, J.W. Kysar, J. Hone, Measurement of the Elastic Properties and Intrinsic Strength of Monolayer Graphene, Science 321(5887) (2008) 385.
[2] J.S. Bunch, A.M. van der Zande, S.S. Verbridge, I.W. Frank, D.M. Tanenbaum, J.M. Parpia, H.G. Craighead, P.L. McEuen, Electromechanical Resonators from Graphene Sheets, Science 315(5811) (2007) 490.
[3] S. Ghosh, I. Calizo, D. Teweldebrhan, E.P. Pokatilov, D.L. Nika, A.A. Balandin, W. Bao, F. Miao, C.N. Lau, Extremely high thermal conductivity of graphene: Prospects for thermal management applications in nanoelectronic circuits, Appl. Phys. Lett. 92(15) (2008) 151911.
[4] A.A. Balandin, S. Ghosh, W. Bao, I. Calizo, D. Teweldebrhan, F. Miao, C.N. Lau, Extremely High Thermal Conductivity of Graphene: Experimental Study, arXiv:0802.1367 (2008).
[5] K.S. Novoselov, A.K. Geim, S.V. Morozov, D. Jiang, M.I. Katsnelson, I.V. Grigorieva, S.V. Dubonos, A.A. Firsov, Two-dimensional gas of massless Dirac fermions in graphene, Nature 438 (2005) 197.
[6] Z. Chen, Y.-M. Lin, M.J. Rooks, P. Avouris, Graphene nano-ribbon electronics, Physica E Low Dimens Syst Nanostruct. 40(2) (2007) 228-232.
[7] T. Takahashi, K. Sugawara, E. Noguchi, T. Sato, T. Takahashi, Band-gap tuning of monolayer graphene by oxygen adsorption, Carbon 73 (2014) 141-145.
[8] V.J. Surya, K. Iyakutti, H. Mizuseki, Y. Kawazoe, Tuning Electronic Structure of Graphene: A First-Principles Study, IEEE Transactions on Nanotechnology 11(3) (2012) 534-541.
[9] H. Zhang, E. Bekyarova, J.-W. Huang, Z. Zhao, W. Bao, F. Wang, R.C. Haddon, C.N. Lau, Aryl Functionalization as a Route to Band Gap Engineering in Single Layer Graphene Devices, Nano Lett.

11(10) (2011) 4047-4051.
[10] T. Sainsbury, M. Passarelli, M. Naftaly, S. Gnaniah, S.J. Spencer, A.J. Pollard, Covalent Carbene Functionalization of Graphene: Toward Chemical Band-Gap Manipulation, ACS Applied Materials & Interfaces 8(7) (2016) 4870-4877.
[11] L. Liao, H. Peng, Z. Liu, Chemistry Makes Graphene beyond Graphene, J. Am. Chem. Soc. 136(35) (2014) 12194-12200.
[12] S. Nakaharai, T. Iijima, S. Ogawa, S. Suzuki, S.-L. Li, K. Tsukagoshi, S. Sato, N. Yokoyama, Conduction Tuning of Graphene Based on Defect-Induced Localization, ACS Nano 7(7) (2013) 5694-5700.
[13] G. Bottari, M.A. Herranz, L. Wibmer, M. Volland, L. Rodriguez-Perez, D.M. Guldi, A. Hirsch, N. Martin, F. D'Souza, T. Torres, Chemical functionalization and characterization of graphene-based materials, Chem. Soc. Rev. 46(15) (2017) 4464-4500.
[14] P. Vecera, K. Edelthalhammer, F. Hauke, A. Hirsch, Reductive arylation of graphene: Insights into a reversible carbon allotrope functionalization reaction, Phys. Status Solidi B 251(12) (2014) 2536-2540.
[15] J.M. Englert, C. Dotzer, G. Yang, M. Schmid, C. Papp, J.M. Gottfried, H.-P. Steinruck, E. Spiecker, F. Hauke, A. Hirsch, Covalent bulk functionalization of graphene, Nat. Chem. 3(4) (2011) 279-286.
[16] J.M. Englert, K.C. Knirsch, C. Dotzer, B. Butz, F. Hauke, E. Spiecker, A. Hirsch, Functionalization of graphene by electrophilic alkylation of reduced graphite, Chem. Commun. 48(41) (2012) 5025-5027.
[17] A. Hirsch, J.M. Englert, F. Hauke, Wet Chemical Functionalization of Graphene, Acc. Chem. Res. 46(1) (2013) 87-96.
[18] K.C. Knirsch, J.M. Englert, C. Dotzer, F. Hauke, A. Hirsch, Screening of the chemical reactivity of three different graphite sources using the formation of reductively alkylated graphene as a model reaction, Chem. Commun. (Cambridge, U. K.) 49(92) (2013) 10811-10813.
[19] V. Strauss, R.A. Schäfer, F. Hauke, A. Hirsch, D.M. Guldi, Polyhydrogenated Graphene: Excited State Dynamics in Photo- and Electroactive Two-Dimensional Domains, J. Am. Chem. Soc. 137(40) (2015) 13079-13086.
[20] R.A. Schäfer, D. Dasler, U. Mundloch, F. Hauke, A. Hirsch, Basic Insights into Tunable Graphene Hydrogenation, J. Am. Chem. Soc. 138(5) (2016) 1647-1652.
[21] A.Y.S. Eng, Z. Sofer, Š. Huber, D. Bouša, M. Maryško, M. Pumera, Hydrogenated Graphenes by Birch Reduction: Influence of Electron and Proton Sources on Hydrogenation Efficiency, Magnetism, and Electrochemistry, Chemistry – A European Journal 21(47) (2015) 16828-16838.
[22] K.E. Whitener, Review Article: Hydrogenated graphene: A user's guide, Journal of Vacuum Science & Technology A 36(5) (2018) 05G401.
[23] K.E. Whitener, W.K. Lee, P.M. Campbell, J.T. Robinson, P.E. Sheehan, Chemical hydrogenation of single-layer graphene enables completely reversible removal of electrical conductivity, Carbon 72 (2014) 348-353.
[24] R.A. Schäfer, J.M. Englert, P. Wehrfritz, W. Bauer, F. Hauke, T. Seyller, A. Hirsch, On the Way to Graphane—Pronounced Fluorescence of Polyhydrogenated Graphene, Angew. Chem. Int. Ed. 52(2) (2013) 754-757.
[25] P. Vecera, S. Eigler, M. Kolesnik-Gray, V. Krstic, A. Vierck, J. Maultzsch, R.A. Schafer, F. Hauke, A. Hirsch, Degree of functionalisation dependence of individual Raman intensities in covalent graphene derivatives, Scientific Reports 7 (2017).
[26] J.M. Englert, P. Vecera, K.C. Knirsch, R.A. Schaefer, F. Hauke, A. Hirsch, Scanning-Raman-Microscopy for the Statistical Analysis of Covalently Functionalized Graphene, ACS Nano 7(6) (2013) 5472-5482.
[27] K.C. Knirsch, R.A. Schaefer, F. Hauke, A. Hirsch, Mono- and Ditopic Bisfunctionalization of Graphene, Angew. Chem. Int. Ed. 55(19) (2016) 5861-5864.
[28] F. Hof, R.A. Schaefer, C. Weiss, F. Hauke, A. Hirsch, Novel λ3-Iodane-Based Functionalization of Synthetic Carbon Allotropes (SCAs)-Common Concepts and Quantification of the Degree of

Addition, Chem. - Eur. J. 20(50) (2014) 16644-16651.
[29] D.R. Dreyer, S. Park, C.W. Bielawski, R.S. Ruoff, The chemistry of graphene oxide, Chem. Soc. Rev. 39(1) (2010) 228-240.
[30] A.J. Birch, 117. Reduction by dissolving metals. Part I, Journal of the Chemical Society (Resumed) (0) (1944) 430-436.
[31] A.L. Wilds, N.A. Nelson, A Superior Method for Reducing Phenol Ethers to Dihydro Derivatives and Unsaturated Ketones, J. Am. Chem. Soc. 75(21) (1953) 5360-5365.
[32] S. Pekker, J.P. Salvetat, E. Jakab, J.M. Bonard, L. Forró, Hydrogenation of Carbon Nanotubes and Graphite in Liquid Ammonia, JPC B 105(33) (2001) 7938-7943.
[33] Z. Yang, Y. Sun, L.B. Alemany, T.N. Narayanan, W.E. Billups, Birch Reduction of Graphite. Edge and Interior Functionalization by Hydrogen, J. Am. Chem. Soc. 134(45) (2012) 18689-18694.
[34] W.-K. Lee, J.K.E. Whitener, J.T. Robinson, P.E. Sheehan, Patterning Magnetic Regions in Hydrogenated Graphene Via E-Beam Irradiation, Adv. Mater. 27(10) (2015) 1774-1778.
[35] X. Zhang, Y. Huang, S.S. Chen, N.Y. Kim, W. Kim, D. Schilter, M. Biswal, B. Li, Z. Lee, S. Ryu, C.W. Bielawski, W.S. Bacsa, R.S. Ruoff, Birch-Type Hydrogenation of Few-Layer Graphenes: Products and Mechanistic Implications, J. Am. Chem. Soc. 138(45) (2016) 14980-14986.
[36] H.E. Zimmerman, A Mechanistic Analysis of the Birch Reduction, Acc. Chem. Res. 45(2) (2012) 164-170.
[37] M. Solà, Forty years of Clar's aromatic π-sextet rule, Frontiers in Chemistry 1 (2013) 22.
[38] E. Clar, The aromatic sextet, Wiley-Interscience, London, 1972.
[39] D. Moran, F. Stahl, H.F. Bettinger, H.F. Schaefer, P.v.R. Schleyer, Towards Graphite: Magnetic Properties of Large Polybenzenoid Hydrocarbons, J. Am. Chem. Soc. 125(22) (2003) 6746-6752.
[40] Z. Chen, C.S. Wannere, C. Corminboeuf, R. Puchta, P.v.R. Schleyer, Nucleus-Independent Chemical Shifts (NICS) as an Aromaticity Criterion, Chem. Rev. 105(10) (2005) 3842-3888.
[41] A.D. Zdetsis, E.N. Economou, A Pedestrian Approach to the Aromaticity of Graphene and Nanographene: Significance of Huckel's (4n+2)π Electron Rule, JPC C 119(29) (2015) 16991-17003.
[42] J. Holzwarth, K.Y. Amsharov, D.I. Sharapa, D. Reger, K. Roshchyna, D. Lungerich, N. Jux, F. Hauke, T. Clark, A. Hirsch, Highly Regioselective Alkylation of Hexabenzocoronenes: Fundamental Insights into the Covalent Chemistry of Graphene, Angewandte Chemie International Edition 56(40) (2017) 12184-12190.
[43] P.W. Rabideau, Z. Marcinow, The Birch Reduction of Aromatic Compounds, Organic Reactions (2004).
[44] T.D. Walsh, Reductive fragmentation of 9,9-diarylfluorenes. Concurrent radical anion and dianion cleavage. Electron apportionment in radical ion fragmentations, J. Am. Chem. Soc. 109(5) (1987) 1511-1518.
[45] R.G. Harvey, Metal-Ammonia Reduction of Aromatic Molecules, Synthesis 1970(04) (1970) 161-172.
[46] P.W. Rabideau, The metal-ammonia reduction of aromatic compounds, Tetrahedron 45(6) (1989) 1579-1603.
[47] A.G. Schultz, The asymmetric Birch reduction and reduction-alkylation strategies for synthesis of natural products, Chem. Commun. (14) (1999) 1263-1271.
[48] L. Liao, Z.H. Song, Y. Zhou, H. Wang, Q. Xie, H.L. Peng, Z.F. Liu, Photoinduced Methylation of Graphene, Small 9(8) (2013) 1348-1352.
[49] P.W. Rabideau, The birch reduction of aromatic Compounds, 1992.
[50] F. Banhart, J. Kotakoski, A.V. Krasheninnikov, Structural Defects in Graphene, Acs Nano 5(1) (2011) 26-41.
[51] D.Y. Zubarev, M. Frenklach, W.A. Lester Jr, From aromaticity to self-organized criticality in graphene, PCCP 14(35) (2012) 12075-12078.
[52] M.R. Philpott, Y. Kawazoe, Edge versus interior in the chemical bonding of graphene materials, Phys. Rev. B 79(23) (2009) 233303.
[53] D.Y. Zubarev, X. You, J. McClean, J.W.A. Lester, M. Frenklach, Patterns of local aromaticity in graphene oxyradicals, J. Mater. Chem. 21(10) (2011) 3404-3409.

[54] M. Shafiul Alam, F. Muttaqien, A. Setiadi, M. Saito, First-Principles Calculations of Hydrogen Monomers and Dimers Adsorbed in Graphene and Carbon Nanotubes, J. Phys. Soc. Jpn. 82(4) (2013) 044702.
[55] M. Yang, A. Nurbawono, C. Zhang, R. Wu, Y. Feng, Ariando, Manipulating absorption and diffusion of H atom on graphene by mechanical strain, AIP Advances 1(3) (2011) 032109.
[56] Ž. Šljivančanin, E. Rauls, L. Hornekær, W. Xu, F. Besenbacher, B. Hammer, Extended atomic hydrogen dimer configurations on the graphite(0001) surface, J. Chem. Phys. 131(8) (2009) 084706.
[57] S. Casolo, O.M. Løvvik, R. Martinazzo, G.F. Tantardini, Understanding adsorption of hydrogen atoms on graphene, J. Chem. Phys. 130(5) (2009) 054704.
[58] P.L. de Andres, J.A. Vergés, First-principles calculation of the effect of stress on the chemical activity of graphene, Appl. Phys. Lett. 93(17) (2008) 171915.
[59] K.P. Katin, V.S. Prudkovskiy, M.M. Maslov, Chemisorption of hydrogen atoms and hydroxyl groups on stretched graphene: A coupled QM/QM study, Phys. Lett. A 381(33) (2017) 2686-2690.
[60] J. Wu, W. Pisula, K. Müllen, Graphenes as Potential Material for Electronics, Chem. Rev. 107(3) (2007) 718-747.
[61] G.M. Psofogiannakis, G.E. Froudakis, DFT Study of the Hydrogen Spillover Mechanism on Pt-Doped Graphite, JPC C 113(33) (2009) 14908-14915.
[62] Y. Wang, H.-J. Qian, K. Morokuma, S. Irle, Coupled Cluster and Density Functional Theory Calculations of Atomic Hydrogen Chemisorption on Pyrene and Coronene as Model Systems for Graphene Hydrogenation, JPC A 116(26) (2012) 7154-7160.
[63] E.F. Valeev, T. Daniel Crawford, Simple coupled-cluster singles and doubles method with perturbative inclusion of triples and explicitly correlated geminals: The CCSD(T)R12^{-} model, J. Chem. Phys. 128(24) (2008) 244113.
[64] J. Kerwin, B. Jackson, The sticking of H and D atoms on a graphite (0001) surface: The effects of coverage and energy dissipation, J. Chem. Phys. 128(8) (2008) 084702.
[65] L. Jeloaica, V. Sidis, DFT investigation of the adsorption of atomic hydrogen on a cluster-model graphite surface, Chem. Phys. Lett. 300(1) (1999) 157-162.
[66] P. Federico, F. Iribarne, A First-Principles Study on the Interaction between Alkyl Radicals and Graphene, Chemistry-a European Journal 18(24) (2012) 7568-7574.
[67] M. Pykal, P. Jurecka, F. Karlicky, M. Otyepka, Modelling of graphene functionalization, PCCP 18(9) (2016) 6351-6372.
[68] T.A. Witten, Jr., L.M. Sander, Diffusion-limited aggregation, a kinetic critical phenomenon, Phys. Rev. Lett. 47(19) (1981) 1400-3.
[69] T.A. Witten, L.M. Sander, Diffusion-limited aggregation, Phys. Rev. B 27(9) (1983) 5686-5697.
[70] L.M. Sander, Diffusion-limited aggregation: A kinetic critical phenomenon?, Contemporary Physics 41(4) (2000) 203-218.
[71] Matsushita, Hayakawa, Sawada, Fractal structure and cluster statistics of zinc-metal trees deposited on a line electrode, Phys Rev A Gen Phys 32(6) (1985) 3814-3816.
[72] Ihle, K. Muller, Diffusion-limited fractal growth morphology in thermodynamical two-phase systems, Phys. Rev. Lett 70(20) (1993) 3083-3086.
[73] M. Sone, K. Toriyama, Y. Toriyama, Liquid crystal Lichtenberg figure, Appl. Phys. Lett. 24(3) (1974) 115-17.
[74] B.B. Mandelbrot, The Fractal Geometry of Nature, Freeman, San Francisco, 1982.

Table of Contents

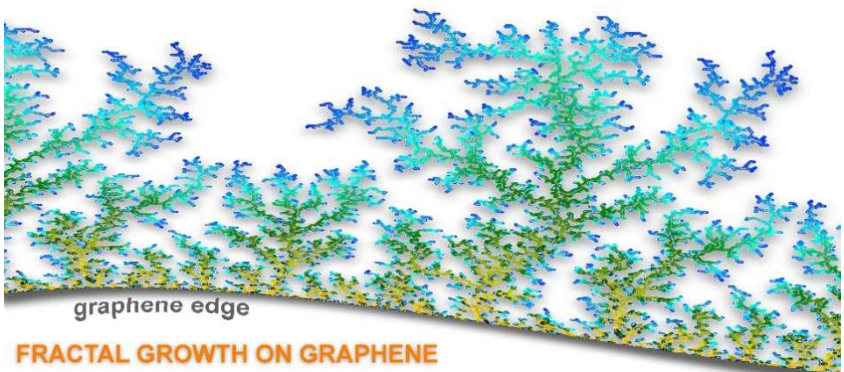

Declaration of interests

☒ The authors declare that they have no known competing financial interests or personal relationships that could have appeared to influence the work reported in this paper.

☐The authors declare the following financial interests/personal relationships which may be considered as potential competing interests: